Nanostructured Li Ion Insertion Electrodes. 2. Tin Dioxide Nanocrystalline Layers and Discussion on "Nanoscale Effect"

P. R. Bueno,* E. R. Leite, T. R. Giraldi, L. O. S. Bulhões, and E. Longo

Interdisciplinary Laboratory of Electrochemistry and Ceramics, Department of Chemistry, Federal University of São Carlos, C. Postal 676, 13565-905 São Carlos, SP, Brazil

Received: February 27, 2003; In Final Form: June 6, 2003

Relaxation processes occurring during electroinsertion into pure SnO_2 and electrochromic SnO_2/Sb were interpreted on the basis of frequency-dependent response models. Within the framework of the classic theory of porous electrodes, the results indicated that, in the case of nanosized particle-based electrodes, the overall kinetic aspects of the insertion process can be controlled by the transport of ionic and electronic species in the liquid and solid phases, respectively. Therefore, if both the electronic and ionic transport are fast in both the solid and liquid phases, or if the state-of-charge is high, a relaxation process corresponding to the insertion of Li^+ in specific sites inside the nanosized particles is clearly identifiable, as foreseen by the model discussed in part 1. As a result, in the SnO_2/Sb samples, we have successfully separated the frequency of slow charging of transport effects due to the nonfaradaic capacitance-related process from that of faradaic related capacitances, because these two processes do not overlap and can, in such specific situations, be separated in complex capacitance diagrams. Moreover, our interpretation of the results indicates that the participation of a large amount of inserted charge in the Sb-doped sample is possible due to the "nanoscale factor", which, allied to the high electronic conductivity in the solid phase, causes rapid charging of the faradaic capacitance-related process. In our interpretation, the faradaic capacitance related process is linked to the insertion of Li^+ into the solid-state phase of nanosized particles and can be interpreted as an ion immobilization or trapping process, as discussed earlier in part 1.

I. Introduction

Nanocrystalline metal oxide electrodes have been incorporated in electrochromic windows[1] and in ion-insertion batteries[2] with significant technological and commercial potentiality. During their operation, electrochromic windows and ion-insertion batteries undergo a common event originating from the insertion of Li^+ ions into the solid-state structure of the host materials, for example, metal oxide electrodes. Despite the geometrical porous effect, this event can be evaluated by frequency-dependent techniques.

Nanoscale range materials have been widely studied for application in energy storage devices due to their distinctive properties, which originate from the presence of large numbers of interfaces, a characteristic that can be exploited to design more efficient devices, including those used for conversion and energy storage. These features allow for several technological applications, mainly in semiconductors and ceramics, depending on the features of the interfaces. Despite these important technological applications, the complex geometry of the electrodes involved in such devices renders any modeling of the transport of Li^+ ions difficult in terms of nanostructured insertion electrodes. This complex situation has only recently begun to be exploited from every standpoint to offer a predictable way to design a wide range of new Li^+ ion insertion electrodes, which might lead to improvements, particularly in the rate capabilities of the electrodes used in communication and remote sensing device batteries.[3]

Still in regard to the use of nanoscale materials in the design of electrodes for Li^+ insertion, it is important to mention specifically the effects of the nanoporous geometry of the electrodes, to which the classic theory of porous electrodes can be applied, as stated in our previous article, Part 1. In an approach based on a situation of porous geometry, the nanostructured material and nanoporous geometry of lithium ion electrodes can dramatically improve the rate capabilities of thin-film dense materials because the distance that Li^+ diffuses in nanostructured electrodes is restricted to the radius of the host material's nanocrystals or to the fibers in nanofiber-based electrodes.[4−6]

The prevailing idea regarding the kinetic reaction of electroinsertion, from the standpoint of Li^+ insertion into the solid state, is that the transport of mobile guests inside the host lattice is the predominant step, with the guests—usually Li^+ ions—moving by ordinary diffusion under semi-infinite conditions. Thus, diffusion is considered the current- and power-limiting step in Li ion insertion electrodes.

In the present paper, we analyze two distinct SnO_2 layers having different nanocrystalline structures and electronic conductivities with the specific purpose of evaluating the influence of these features on the Li^+ charge kinetics, as was stated in part 1 of this article. The charge modes were analyzed on the basis of impedance and complex capacitance responses. Our interpretation of the results indicates that the average size of nanocrystalline particles improves the overall kinetics, because Li^+ diffusion occurs rapidly through the bulk of SnO_2−Sb nanocrystal-based electrodes whose particle sizes are smaller than those of the pure SnO_2 larger size nanoparticle-based

* To whom correspondence should be addressed. E-mail: paulo@iris.ufscar.br.

10.1021/jp034512m CCC: $25.00
Published on Web 08/06/2003

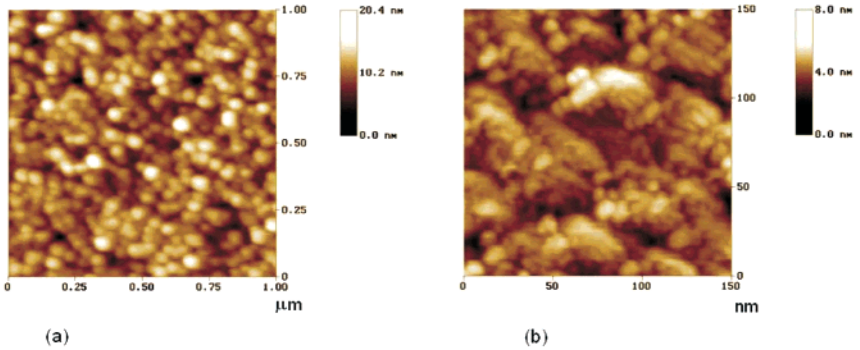

Figure 1. AFM photomicrographs of (a) pure and (b) Sb-doped nanosize particle-based electrodes.

electrodes. This feature also involves an important aspect regarding the interpretation of the frequency-domain response of electrodes. The nanosize particle effect in SnO_2−Sb electrodes, allied to the feature of higher electronic conductivity, also increases the charge capability because the Li^+ guest can access a greater number of sites in the bulk (intercalated sites), since a high electronic charge is available along the electrode to compensate for the inserted Li^+ ions. This entire effect can be evaluated easily through complex capacitance responses.

II. Experimental Section

SnO_2 was chosen as the insertion material owing to its promising use as anode material for lithium batteries, after the announcement, by Fuji Photo Film Celltee Co Ltd., Japan, of the STALION lithium ion cell.[7] Furthermore, at doping levels of about 2−7% antimony, SnO_2 can form degenerate semiconductors displaying high electrical conductivity,[8,9] which may be similarly relevant to the charge capability, as will be discussed later.

The SnO_2 nanocrystalline-based layer was prepared by the dip-coating method, using a sol−gel resin prepared by the polymer precursor method,[10,11] in which tin citrate was used to incorporate metal ions into a rigid organic polymer net formed by a polyesterification reaction between citric acid and ethylene glycol. The SnO_2/Sb thin layer was prepared using 7 mol % Sb.[11] After the deposition of sol−gel layers on glass slides covered with an indium-doped SnO_2 film (ITO) (Donnelly 14 Ω/□), the layers were dried on a hot plate (∼150 °C) and heat treated in two steps. In the first step, the temperature was raised to 300 °C at a heating rate of 1 °C·min^{-1} and kept at this temperature for 2 h to eliminate organic materials. In the second step, the films were heat treated at 550 °C and kept at this temperature for 2 h, using 5 °C·min^{-1} heating and cooling rates.

The crystallization was confirmed by X-ray diffraction (SIEMENS, D5000), using grazing incident angle and Cu Kα radiation. The microstructure was characterized by scanning tunneling microscopy (Digital Instruments-Nanoscope III-A), with the pure SnO_2 sample presenting a mean grain size of 75 nm and the Sb-doped sample showing a value of 13 nm. Figure 1 illustrates the morphology of pure and Sb-doped nanostructures. The electronic resistivity of the films was measured by the four-probe method, presenting the values of >1 and ∼2.6 × 10^{-3} Ω·cm for pure and doped samples, respectively. The SnO_2 films' thickness was determined by SEM (scanning electron microscopy) micrographic analysis (obtained with a ZEISS microscope, model DSM 940A) and was ∼1000 nm for pure and ∼812 nm for Sb-doped SnO_2 films.

Electrochemical experiments were performed with an Autolab PGSTAT20 device equipped with a FRA module. A conventional three-electrode cell setup was used, with the counter electrode consisting of a 1 cm^2 platinum foil. The quasi-reference electrode was a silver wire, and the electrolyte was 0.1 M $LiClO_4$ dissolved in propylene carbonate. The cell was previously purged with dry N_2 gas. The frequency response was measured using an ac potential of 10 mV rms and a frequency scan ranging from 100 kHz to 1 mHz. All the frequency-response data presented in this letter were pretreated to remove the series resistance (R_s) introduced by the solution and ITO substrate.

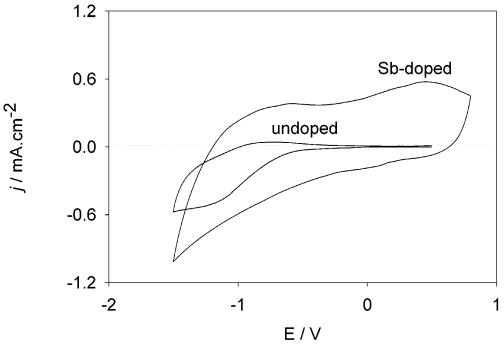

Figure 2. Cyclic voltammograms of the undoped and Sb-doped SnO_2 films in 0.1 M $LiClO_4$ dissolved in propylene carbonate with a silver wire as reference. The potential sweep rate was 50 mV·s^{-1}. The high frequency region is likely being influenced by the start of SEI formation (see section III.F of part 1).

III. Results and Discussions

A. General Electrochemical Features. Figure 2 shows cyclic voltammograms of pure and Sb-doped nanocrystalline SnO_2 films in anhydrous propylene carbonate. The two oxidation−reduction peaks visible in the cathodic and anodic currents correspond to the reduction and oxidation processes of SnO_2 films, and they are attributed, respectively, to lithium insertion and deinsertion. The cathodic and anodic charge densities identified in the cyclic voltammograms are clearly high for doped film and similar to those presented in ref 1. The Sb-doped SnO_2 film displays a higher charge capacity and charge reversibility than the pure film. The characteristic (rectangular) shape of the cyclic voltammogram of the doped sample is typical of systems possessing strong double-layer capacitance at the solid/liquid interface.

The cathodic and anodic charge densities identified in the cyclic voltammograms are −4.2 and 0.52 mC for the pure SnO_2 sample and −18.4 and 16.5 mC for the SnO_2−Sb sample, indicating high charge reversibility at 50 mV·s^{-1} for the Sb-doped sample. The charge reversibility, which is dependent on several kinetic aspects of the electrodes, will be discussed in greater detail in this paper.

B. Frequency-Dependent Response: Capacitance and Impedance. Figure 3 depicts the complex plane impedance (Z^*

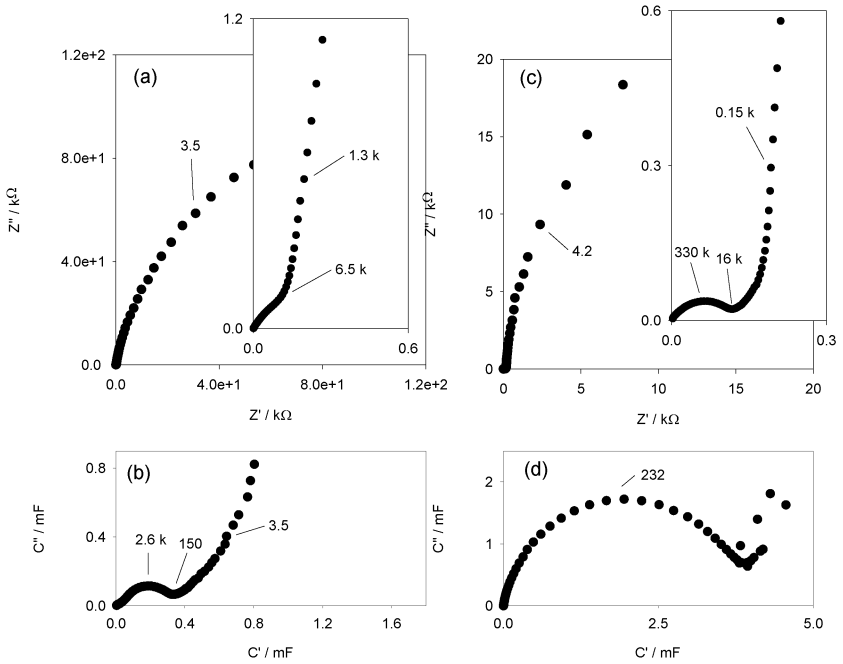

Figure 3. Impedance (Z^*) and capacitance (C^*) complex plane plots for the SnO_2 films in a solution 0.1 M $LiClO_4$ in propylene carbonate with a silver wire as reference. Undoped sample: (a and b) at −100 mV. Sb-doped sample: (c and d) at 0 V. All the indicated frequencies are in millihertz.

$= Z' + iZ''$) and capacitance ($C^* = C' + iC''$) plots in two steady-state conditions for the pure and Sb-doped SnO_2 nanocrystalline layers, respectively. The insets also show high-frequency responses identified in the impedance plots. The most noteworthy point revealed by the capacitance plots is that the response of the Sb-doped film is evidenced mainly by a unique, well-defined relaxation process (better described as a Havriliak−Negami relaxation process[12]), despite its more positive steady-state potential. This suggests that the charge is the manifestation of a predominant phenomenon that can be interpreted, in principle, in terms of the large bulk inserted charge, as previously described in part 1. The responses of the Sb-doped film indicate that a large amount of the inserted charge participates in a solid-state reaction process, which can be described as the occupancy of an ionic trapping process, in line with the expected response of the high state-of-charge of nanostructured electrodes analyzed in part 1 (Figure 6 of part 1 with $C_b = 10C_{dl}$ and $C_b = 10^2C_{dl}$). A similar response was experimentally evidenced in ref 13, using a modulated transmittance technique in nonporous electrodes. However, it is important to point out that, in the aforementioned case, both capacitances are bulk-related while, in the present case, only the capacitance relating to the low charging process is really a bulk capacitance. In ref 13, the ionic trapping response is assumed to be associated with the coloration mechanism in electrochromic *a*-WO_3.[13] In the present case, the low charging process capacitance is also expected to be related to the coloration mechanism, as will be discussed further, but the fast charging capacitance represents the nonfaradaic capacitance of the double-layer effects in the porous channels of the nanostructured electrode.

The effects of some kinds of transport phenomena are expected, possibly at high frequencies. These effects are difficult to observe in a capacitance representation, but they are clearly visible in an impedance plot. Undoped samples, for instance, yield an impedance shape that can be viewed in the high-frequency wing, such as the expected Warburg-like pattern (see inset of Figure 3a). This pattern reflects the transport features involved mainly in electron diffusion since, in the present case, the mobility of the electrons is lower than that of the inserted ions, as presumed by refs 1 and 14. Thus, a similar response occurs to that foreseen by charging in the presence of simple transport, as described in section III.B (Figure 5) of part 1. In the pure SnO_2 sample, electron mobility is expected to be lower than Li^+ mobility in the electrolyte phase because of the depletion layer existing between the SnO_2 semiconductor particles. Therefore, both a lower donor concentration and an electron-depleted space charge layer at the surface are responsible for a potential drop throughout the thickness of the solid phase, resulting in a transport effect that strongly overlaps and predominates over the slow bulk charging process. Note that in the case of the responses of Figures 3 and 4 the influence of the solid electrolyte interface (SEI) is neglected, since SEI pronounced formation is expected to occur at higher potential (>2 V on the Li/Li^+ scale).

The contribution of Sb doping consists of Sb-doping atoms, which can increase the electronic density (particularly at levels exceeding 4 mol %), inducing highly electronic conductivities that contribute to decrease the electron-depleted effect at the surface of nanoparticles, possibly helping to increase the overall charging. Therefore, Sb doping decreases the resistivity of specific space charge regions. The lesser effect of the space charge region may result in additional electronic conductivity, which contributes to the overall charging in addition to the "nanoscale effect".

It can be noted that the rate-determining step is electronic compensation of the charging of the double layer, due to the fact that Li^+ solvated ions are highly mobile in the pores. As stated in part 1 of this paper, the insertion kinetics is dependent on the C_{dl}. However, C_{dl} is a value distributed throughout the layer's thickness and depends on the potential drop in the SnO_2 solid phase. Therefore, if the donor density increases in the solid phase, a fast C_{dl} charging with a rapid access of C_{dl} sites is expected, as stated in eq 17 of part 1. In other words, when fast electronic transport occurs in addition to the "nanoscale effect", all the insertion sites can be easily accessed because the

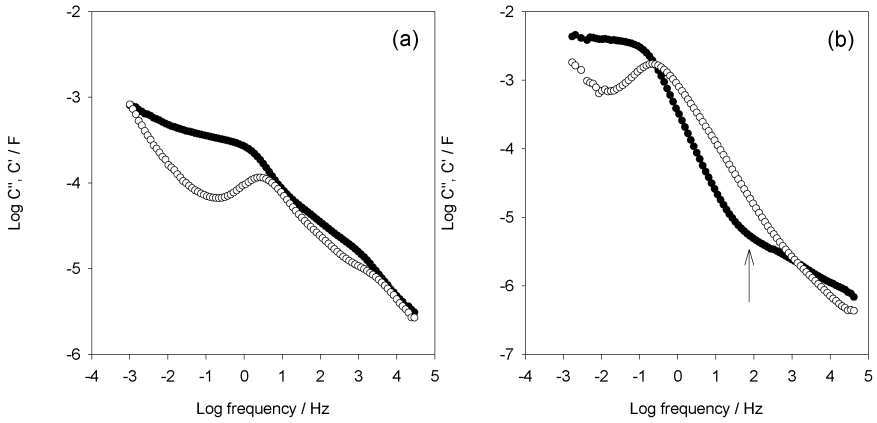

Figure 4. Capacitance spectra for the SnO_2 films in a solution of 0.1 M $LiClO_4$ in propylene carbonate with a silver wire as reference. (a) Undoped sample at −100 mV, (●) real and (○) imaginary parts. (b) Doped sample at 0 V, (●) real and (○) imaginary parts. The arrow in part b indicates the frequency of change between the diffusional and trapping regimes.

electronic charge can rapidly compensate the ionic charge. It is important to keep in mind that the "nanoscale effect" implies a very short diffusion length, as in the case of SnO_2−Sb doped film (a mean diffusion length of 6.5 nm for a mean particle size of 13 nm, as determined by AFM). Thus, as stated in part 1, a solely pure capacitive response is capable of representing the Li^+ charge in the host structure.

Consequently, in the impedance response of the doped sample, the high-frequency range of the impedance plot displays yet another behavior; that is, an arc rather than a ∼45°-inclined line is visible (see insets of Figure 3c). If we now recall the simulations previously discussed (see Figure 5c and d in part 1), which correspond to impedance plots of transport in different types of state-of-charge of nanostructured electrodes, it can be observed that, in those cases, an arc develops in the high-frequency wing of the spectra, and a "blocking" effect dominates at low frequencies. The impedance plots in the insets of Figure 3c reproduce this pattern to some extent, but due to the fact that the responses are actually more complex than simple arcs, it seems evident that the effect of some electronic transport (or a mixture of electronic and ionic transport contributions) must be considered in the high-frequency region. Therefore, a transmission line circuit with distributed resistance in the solid phase describes the response better than the pure capacitive elements, $C_{dl} + C_b$.

In other words, although the electronic transport is fast in the Sb-doped sample, some influence is observed at high frequencies due to the influence of solid electrolyte interface (SEI) formation, as discussed in section III.F of part 1. However, in the former situation, the effect of electronic transport on the frequency response is much less pronounced than that on the pure SnO_2 nanostructured electrode. This feature, allied with the higher state-of-charge easily reached in the Sb-doped sample, allows one to separate $C_{dl} + C_b$ in the complex capacitance diagram of Figure 4. As a result, the Sb-doped feature is determined exclusively by a *trapping-like response*. This clearly indicates that the dynamics of electronic transport and the insertion reaction effect are separated in the Sb-doped sample, reinforcing the occurrence of fast overall charging of this electrode. In fact, this is the situation expected that explains the high performance of nanostructured electrodes during charge and discharge processes.

Accordingly, we can properly determine $C_{dl} \sim 4.6\ \mu F$ as the capacitance value corresponding to the elbow (at 120 Hz) that signals the transition from fast surface states to trapping-like bulk regimes (see arrow in Figure 4b). The total value of the capacitance can be readily determined from the low-frequency limit of C', resulting in a total capacitance of $C_t = 4.5$ mF, 3 orders of magnitude greater than C_{dl}. Therefore, the trapping-like capacitance C_b represents the predominant effect of the film charge, and as was theoretically discussed in part 1, the fact that C_b by far exceeds C_{dl} indicates that ions at the surface of nanoparticles can be seen as a relay from the solution bulk to insertion sites and on into the nanoparticle bulk. It is important to point out here that the value of C_{dl} lies within the magnitude expected for a double-layer capacitance.

The undoped sample, on the other hand, shows a very different picture (see Figure 3a and b): a double contribution to the capacitance in the frequency range below 10 Hz. In this case, the charging effect of insertion sites (trapping-like) is lower due to high resistance to electronic transport in the solid phase. The electronic transport therefore dominates the overall response in a wide frequency window, precluding the above-described separation procedure for the doped sample. Hence, it is impossible to signal a clear change of behavior in the C' spectra (see Figure 4a); moreover, the capacitance does not stabilize at a value corresponding to the contribution of the Li^+ ions in the bulk, C_b. This behavior is similar to that represented in Figure 7 of part 1, where $C_b = 0.1C_{dl}$. Thus, the $C_{dl} > C_b$ or $C_{dl} \sim C_b$ response is expected to exist when electronic transport is hindered in the solid phase. A most likely cause of the difference in charge reversibility observed in Figure 2 is the differences in electronic resistance observed in the solid phase of Sb-doped and undoped samples. Moreover, the mixed behavior at frequencies below 10 Hz presumably indicates that electronic transport does not occur as rapidly as that in the case of the doped sample. The low-frequency limit of the capacitance is equal to $C_t = 0.81$ mF, that is, about 5-fold lower than that in the Sb-doped sample.

As discussed above, the charging efficiency can be improved by electronic doping of the nanostructured host. The state-of-charge also has the effect of increasing the donors in the solid phase, which helps to decrease the potential drop. Therefore, in porous electrodes composed of nanoparticles, the thickness of this depletion layer can vary with the electrode potential, that is, the charge injected into the electrode.[15] However, in higher doped nanoparticle-based electrodes, the depletion layer is expected not to vary much, since the electrode potential decreases with the injection of electrons. This is expected because, with a higher donor concentration in highly doped nanostructured hosts, the depletion layer does not offer a significant resistance to electronic transport.

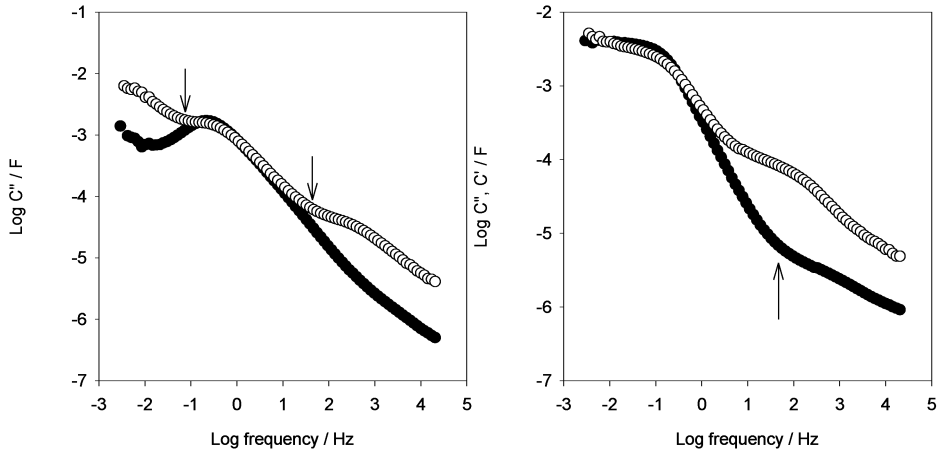

Figure 5. Capacitance spectra for the SnO_2/Sb films in a solution of 0.1 M $LiClO_4$ in propylene carbonate with a silver wire as reference. (a) Imaginary part of the SnO_2/Sb sample at (●) 0 mV and (○) −100 mV. Real part of the SnO_2/Sb sample at (●) 0 mV and (○) −100 mV. The arrow in part b indicates the frequency of change between the diffusional and trapping regimes.

If one considers that the impedance response of an Sb-doped film resembles that of a trapping scheme, the resistance to Li^+ insertion or trap is R_{ct}, as stated in part 1, and transitions exist between double-layer surface sites and bulk sites. Because diffusion occurs rapidly in the Sb-doped sample, the Li^+ guest easily accesses the intercalation sites, increasing this sample's charge capability, with the surface sites acting as fast charge state and the trap or intercalation sites as slow charge state. This interpretation is congruent with the fact that the ion-trapping process relates to the coloring centers in electrochromic *a*-WO_3[13] and with the fact that the electrochromism of the SnO_2/Sb electrode is fully reversible and very stable.[1] In fact, the coloration and decoloration processes of SnO_2/Sb electrodes are very fast[1] and the switching speed is even faster.

With regard solely to the aspect of electroinsertion, involving the insertion of mobile guest ions from an electrolyte into the structure of a solid host, experimental evidence reveals the presence of different capacitive components in nanostructured insertion compounds (in which the low-frequency capacitive behavior is greater than the high-frequency capacitance associated with the Warburb impedance). This behavior at low frequencies can be attributed to the fact that a substantial percentage of Li^+ guests spend most of their time located in the structure rather than in the liquid phase. As a result, the overall response can be interpreted as an ionic trapping scheme, in which the ions from the solution are immobilized in the host structure as a result of solid-state charge transfer (see part 1).

In a situation of high state-of-charge, because the guests spend most of their time localized, one can consider that the C_b capacitance reflects the electrochromic performance of the device, since the electrons are also localized to compensate for the localized ionic charge in the bulk, which contributes to the coloring process. In other words, the dynamics of electrons follows almost completely the dynamic of ions in a high state-of-charge, because electron states are introduced, for instance, into empty d band states to compensate for occupied ionic states (immobilized or trapped ionic Li^+ charge), where Li^+ can form a bond for bridging-like oxygen adjacent to the reduced metal atoms in the host structure.

C. More Difficult To Access Sites. As described in part 1, the host can contain more than one insertion site. Therefore, the capacitance may not be limited to the value of $C_{dl} + C_b$ associated with the fast and slow transport states, as described in part 1. On a sufficiently long time scale, a larger amount of charge than that considered in Figure 4 can be monitored by a small potentiostatic increase dV, so that the system's capacitance is expected to increase owing to the possibility of Li^+ enriching the more difficult to access sites, such as the tetragonal sites. Actually, it is likely that a "sea" of fast charge sites acts as a source of Li^+ ion in the bulk of the host where the solid-state reaction (homogeneous charge transfer) occurs.

As can be seen in Figure 3c and d, another very slow charging process, which is not, in principle, associated with the coloring process, is visible[13] in the low-frequency region, similar to that observed in ref 13.

Figure 5 illustrates the above-described situation more clearly. This figure shows the complex capacitance response of the SnO_2-doped sample in two distinct state-of-charge situations. When the charge is increased by altering the system's steady state, the low and high frequencies are altered as a consequence of electron insertion and of the manifestation of another more difficult to access site. These more difficult to access sites alter the nature of the relaxation response, complicating the analysis, particularly if their relaxation frequencies differ even slightly from those of the previous fully occupied site. However, the possible manifestation of a new more difficult to access intercalation site does not change the previous dominant process at intermediate frequencies, as illustrated by the arrows in Figure 5a, which shows the response of C'' as a function of frequency.

Moreover, the responses are congruent with what was discussed in part 1, indicating that, at least in SnO_2/Sb films, a large part of the inserted charge participates in the ion-trapping process (solid-state react ion). Furthermore, in Sb-doped films, the relaxation process is predicted to occur mainly because of the "nanoscale effect", which eliminates the influence of the diffusion resistance in the response.

D. Some Aspects of the Particles' Surface. Another important aspect to mention is the difference in nanosizes between the Sb-doped and the undoped samples. If one considers a disordered surface layer of 2 nm[16] on each particle in our samples, the disordered layer of each particle in the Sb-doped sample represents 39.4% of the total volume for a mean grain size of 13 nm, while, in the pure SnO_2 sample, it represents only 0.8% for a mean grain size of 75 nm.

An intermediate disordered phase therefore exists between the nanoparticle's core and electrolyte surface states. On one hand, this disordered phase can contribute to the formation of a SEI at high cathodic or anodic potentials. On the other hand, for instance in the Sb-doped sample presented here, although the SEI effect is neglected, this phase represents much of the

volume of the electrode and has the effect of increasing the porous volume in a similar proportion, improving the connected "sea" effect of fast charge sites (nonfaradaic process). These sites can therefore rapidly become filled, and the ions subsequently access the slow charge "lake" sites in the core. In such a situation, interfacial density is also an important factor that contributes to the charge capacity and the kinetics of the electroinsertion reaction in nanostructured devices. A more detailed analysis of this aspect, including experiments involving the contribution of the SEI, will be discussed in future reports.

IV. Final Remarks and Conclusions

In summary, it has been established that the immobilization or trapping of ionic species is the determinant effect in SnO_2/Sb samples. A large portion of charge participates in this process (trapping charge), with nonfaradaic balanced surface charges presumably representing less than 0.1% of the total charge. One can therefore conclude that the charge process is improved because of the high electronic and ionic conductivity. The Sb-doped atoms supply greater electronic conductivity, while the "nanoscale effect" provides the rapid ionic insertion into the nanostructured particles. This situation not only allows more sites (e.g., those causing ionic trapping) to be accessed but also increases the rate and reversibility of the overall insertion process.

The results of the higher electronic conductivity allied to the "nanoscale effect" can be explained from the viewpoint of the relaxation behavior of doped samples, which clearly differs from that of undoped samples. It could be inferred that, in the Sb-doped sample, the intercalation sites become charged more rapidly due to the existence of fast electronic transport, which reduces the influence of the potential drop throughout the layer's thickness. In other words, when the diffusion does not limit the Li^+ transport because such a limitation is overcome by the "nanoscale effect" of the nanostructured insertion electrode, the donor concentration in the solid phase becomes a very important factor of the electrode's performance.

According to refs 4−6, a nanostructured SnO_2-based anode prepared by template synthesis has improved rate capabilities. The explanation these references give is based on the fact that the distance that Li^+ must diffuse in the solid state is shorter than the distance it has to diffuse in a microstructured electrode,[4−6] an observation that reinforces the conclusions derived from our analysis based on frequency-dependent responses in nanostructured electrodes.

Acknowledgment. The financial support of this research project by the Brazilian research funding agencies FAPESP and CNPq is gratefully acknowledged. Special thanks are due to Ms. Beatrice Allain for her grammatical correction of this text in LATEX format.

References and Notes

(1) zum Felde, U.; Haase, M.; Weller, H. *J. Phys. Chem. B* **2000**, *104*, 9388.
(2) Tarascon, J.-M.; Armand, M. *Nature* **2001**, *414*, 359.
(3) Nagasubramanian, G.; Jungst, R. G. *J. Appl. Electrochem.* **2001**, *31*, 99.
(4) Martin, C. R.; Li, N.; Scrosati, B. *J. Power Sources* **2001**, *97*−*98*, 240.
(5) Li, N.; Martin, C. R.; Scrosati, B. *Electrochem. Solid-State Lett.* **2000**, *3*, 316.
(6) Li, N.; Martin, C. R. *J. Electrochem. Soc.* **2000**, *148*, A164.
(7) European Patent 0,6651,450, A1 (1995).
(8) Koch, H. *Phys. Status Solidi* **1963**, *3*, 1059.
(9) Shanthi, E.; Dutta, V.; Banerjee, A.; Chopra, K. L. *J. Appl. Phys.* **1980**, *51*, 6243.
(10) Kakihana, M. *J. Sol*−*Gel Sci. Technol.* **1996**, 6, 7.
(11) Bernardi, M. I. B.; Barrado, C. M.; Soledade, L. E. B.; Leite, E. R.; Longo, E. *J. Mater. Sci.: Mater. Electron.* **2002**, *13*, 403.
(12) Bottcher, C. J. F. *Theory of Electric Polarization*; Elsevier: Amsterdam, 1978.
(13) Bueno, P. R.; Garcia-Belmonte, G.; Fabregat-Santiago, F.; Bisquert, J. Submitted for publication.
(14) Kulesza, P. J.; Cox, J. A. *Electroanalysis* **1998**, *10*, 73.
(15) Boschloo, G.; Fitzmaurice, D. *J. Phys. Chem. B* **1999** *103*, 3093.
(16) Dieguez, A. V. A.; Romano-Rodregues, A.; Morante, J. R. *J. Appl. Phys. Chem.* **2001**, *90*, 1550.